The Cr local structure in epitaxial $CrPt_3$(111) films probed using polarized x-ray absorption fine structure

2005 J. Phys.: Condens. Matter 17 2529

(http://iopscience.iop.org/0953-8984/17/17/001)

INSTITUTE OF PHYSICS PUBLISHING JOURNAL OF PHYSICS: CONDENSED MATTER

J. Phys.: Condens. Matter **17** (2005) 2529–2541 doi:10.1088/0953-8984/17/17/001

The Cr local structure in epitaxial $CrPt_3(111)$ films probed using polarized x-ray absorption fine structure

M Maret[1,6], F Bley[1], C Meneghini[2,3], M Albrecht[4], J Köhler[4], E Bucher[4] and J L Hazemann[5]

[1] Laboratoire de Thermodynamique et Physico-Chimie Métallurgiques, CNRS/INPG/UJF, BP 75, 38402 Saint-Martin d'Hères, France
[2] Dipartimento di Fisica Universitá di 'Roma Tre' Via della Vasca Navale 84 I-00146 Roma, Italy
[3] INFM-OGG c/o ESRF Grenoble, France
[4] Department of Physics, University of Konstanz, PO Box M621, D-78457 Konstanz, Germany
[5] Laboratoire de Cristallographie, CNRS, BP 166, 38042 Grenoble, France

E-mail: mireille.maret@ltpcm.inpg.fr

Received 6 January 2005, in final form 17 March 2005
Published 15 April 2005
Online at stacks.iop.org/JPhysCM/17/2529

Abstract

The local atomic structure of $CrPt_3(111)$ thin films grown by molecular beam epitaxy at different temperatures (400 and 850 °C) has been investigated by polarized x-ray absorption spectroscopy (XAS) at the chromium K edge. Previous x-ray diffraction and magnetic studies have revealed that films grown at 850 °C present the $L1_2$ chemically long range ordered structure and are ferrimagnetic with the occurrence of perpendicular magnetic anisotropy (PMA). In contrast, films grown at 400 °C, which are non-magnetic, do not show any indication of $L1_2$-type long range order. From the polarization dependence of XAS, different chemical orders in the film plane and perpendicular to it are reported for the non-magnetic film: Cr absorbers are surrounded by only Pt atoms in the film plane while out of the film plane Cr nearest neighbours are observed. The higher deposition temperature of the ferrimagnetic film (850 °C) leads to a more isotropic structure reducing the Cr–Cr out-of-plane correlations, as expected from the $L1_2$ ordered structure. These findings show that ferrimagnetism in $CrPt_3$ films is strongly sensitive to the Cr–Cr correlations. Furthermore, the remaining in-plane tensile deformation found in the ferrimagnetic film is too small for yielding the observed PMA. It is suggested that the strong PMA originates from the ferromagnetic coupling between Cr second-nearest neighbours lined up along the ⟨001⟩ directions and which develop an orbital moment parallel to the spin moment as found by relativistic energy band calculations.

[6] Author to whom any correspondence should be addressed.

1. Introduction

Over the last ten years a considerable effort has been devoted to T–Pt (T = Cr, Fe and Co) magnetic alloy films, as potential media for high density perpendicular recording [1–4]. The occurrence of perpendicular magnetic anisotropy (PMA) in ferromagnetic films is closely related to chemical ordering characterized by T–Pt (T–T) bonds preferentially perpendicular (parallel) to the film plane. The extent of such ordering is either on a long range as observed in $L1_0$ ordered FePt(001) films or on a short range as for instance in fcc disordered $CoPt_3(111)$ films [5]. For the latter, angle-dependent x-ray magnetic circular dichroism measurements revealed the microscopic origin of magnetocrystalline anisotropy which was correlated with the selective hybridization along the film normal between Co atoms with a large magnetic moment and Pt atoms with a large spin–orbit (SO) coupling [6]. The ferrimagnetic $L1_2$ ordered $CrPt_3(111)$ films obtained by co-deposition using molecular beam epitaxy [7] or after annealing Cr/Pt multilayers [8] develop high PMA. The origin of PMA in $CrPt_3(111)$ films is more subtle than in $CoPt_3(111)$, because the local order in the $L1_2$ structure is perfectly isotropic. In ferromagnetic $CoPt_3(111)$ films, PMA vanishes effectively with the appearance of $L1_2$ ordering. In ordered $CrPt_3(111)$ films, it is suggested that PMA is rather a consequence of the ferrimagnetic order between Cr and Pt nearest neighbours than induced by the residual out-of-plane compressive strain. The magnetization process is effectively driven by the ferromagnetic coupling between Cr atoms which have an orbital moment parallel to the large spin moment ($\mu_s(\mathrm{Cr}) = 3.37\ \mu_\mathrm{B}$ to be compared with $\mu_s(\mathrm{Pt}) = -0.26\ \mu_\mathrm{B}$) due to the spin–orbit coupling of Pt, as shown by theoretical calculations [9]. Indeed, the six Cr neighbours at a distance a from a Cr atom located in the (111) plane (a being the fcc lattice constant) are along the $\langle 001 \rangle$ directions making an angle of 54.74° with the [111] growth direction, and this arrangement would favour an easy axis of magnetization perpendicular to the film plane. This interpretation is supported by the fact that the magnetic anisotropy energy measured in a $CrPt_3(001)$ film grown on MgO(001) is very close to the shape anisotropy [7], in spite of the existence of an in-plane compressive strain. Therefore, the compressive strain-induced uniaxial magnetic anisotropy, which was in the plane for $CrPt_3(110)$ films grown on MgO(110) and out of the plane for $CrPt_3(111)$ textured films grown on SiN, is not convincing [10]. Indeed, for $CrPt_3(110)$ films the two directions, [001] and $[1\bar{1}0]$, are not equivalent with respect to the two nearest Cr–Cr distances which are respectively equal to a and $\sqrt{2}a$. X-ray absorption fine structure (XAFS) analysis is known to be a powerful technique for selectively probing the details of the local atomic structure around a specific atom in the sample. In addition, the linear polarization of synchrotron radiation, coupled with the directional dependence of the photo-absorption process (polarized XAFS), allows probing the structural features along specific directions in the samples [11]. In this study, the possibility offered by the polarized XAFS technique was exploited to probe in epitaxial $CrPt_3$ films segregation effects and chemical order developed during growth. The analysis of XAFS data collected at the Cr K edge as a function of the angle between the x-ray beam linear polarization and the film plane allowed us to study in detail the local atomic environment around Cr atoms in the (111) film plane and perpendicular to it.

2. Experimental technique

X-ray absorption spectroscopy (XAS) measurements were performed for two (111)-oriented $CrPt_3$ films on the CRG BM32 beam line at the European Synchrotron Radiation Facilities (ESRF, Grenoble). $CrPt_3$ films were prepared by co-deposition from two e-beam sources using molecular beam epitaxy. Two films with a thickness of ∼470 Å were grown at 400 and 850 °C

on a seed layer of 50 Å Pt, previously deposited at 650 °C on (0001)-oriented Al_2O_3 substrates. A protective cap layer of 20 Å Ru was deposited on each sample. The film grown at 850 °C develops an $L1_2$ long range order characterized by a chemical order parameter of 0.95 (close to 1, the value for a perfectly $L1_2$ ordered film) and a strong uniaxial magnetic anisotropy ($K_u = 0.27$ MJ m^{-3}), as previously reported [7]. In contrast, the film grown at 400 °C adopts a fcc structure chemically disordered at long range and is non-magnetic. The XAS spectra were collected at the Cr K edge ($E_0 = 5993$ eV) using a total electron yield set-up [12]. To avoid the Bragg peaks of the substrate, the samples were mounted on a 360° rotating plate. For each film, two spectra were collected at room temperature corresponding to the in-plane ($111_\parallel$) and out-of-plane ($111_\perp$) polarizations. For the $111_\parallel$ geometry the rotating plate was inclined at 8° from the horizontal position (the electric field vector **E** being strictly in the film plane); for the $111_\perp$ geometry the sample plate (after a rotation of 90° around the incoming beam) was vertical and **E** was at 8° to the surface normal. In the following, we label the in-plane polarization data with $400_\parallel$ and $850_\parallel$ and the out-of-plane polarization data with $400_\perp$ and $850_\perp$ for the two samples.

The experimental XAS spectra, $\mu(E)$, were treated following the standard methods to extract the XAFS structural signal $\chi(k)$: the pre-edge background was fitted with a straight line and subtracted; the post-edge atomic background was modelled with a smooth polynomial spline through the experimental data. The energy scale for the photoelectron wavevector ($k = \hbar^{-1}\sqrt{2m(E - E_0)}$) was defined choosing the edge energy (E_0) at the maximum of the $\mu(E)$ first derivative. The statistical noise of XAS data (η) was evaluated as follows: the post-edge experimental data were fitted with high order polynomials simulating the structural signal, then the statistical noise was estimated as the variance of the difference, normalized to the jump height between polynomial functions and the experimental data. Values of η have been found to be in the range of 1–3 $\times 10^{-3}$.

Quantitative analysis of XAFS spectra has been performed fitting the k-weighted experimental data $k\chi(k)$ to the standard XAFS formula [11]:

$$k\chi_{th}(k) = S_0^2 \sum_j \frac{N_j}{R_j^2} F_j(k) \exp(-2k^2\sigma_j^2) \exp\left(-\frac{2R_j}{\lambda(k)}\right) \sin(2kR_j + \phi_j(k)) \quad (1)$$

where N_j is the multiplicity of the jth contribution, $2R_j$ and σ_j are respectively the average length and variance (Debye–Waller factor) of the photoelectron path. $F_j(k)$ and $\phi_j(k)$ are the amplitude and phase shift functions. $\lambda(k)$ is the photoelectron mean free path and S_0^2 is an empirical parameter taking into account many-body effects. Dealing with a non-isotropic structure, an effective multiplicity number, $\tilde{N}_j$, must be used [11] instead of N_j. $\tilde{N}_j$ takes into account the polarization dependence of the photo-absorption process and single-scattering processes; it is given by [13]

$$\tilde{N}_J = 3 \sum_{i=1}^{N_j} \cos^2 \alpha_{ji} \quad (2)$$

where α_{ji} is the angle between the x-ray polarization vector and the bond direction between the absorbing atom and the ith scatterer in the jth shell.

Table 1 summarizes the signals, SS_i, used in the analysis, emphasizing the different sensitivities in the two geometries employed. The scattering paths between the central atom Cr_0 and its ith neighbours, Pt_i and Cr_i, associated with these signals are schematized in figure 1. The $111_\perp$ geometry selectively probes out-of-plane contributions; thus the $400_\perp$ and $850_\perp$ polarized XAFS signals come from the neighbours located out of the film plane ($\tilde{N}_\perp^{in} = 0$ in table 1). In contrast, the $111_\parallel$ geometry probes in-plane and out-of-plane contributions; thus the $400_\parallel$ and $850_\parallel$ polarized XAFS data are a combination of in-plane ($\tilde{N}_\parallel^{in}$) and out-of-plane

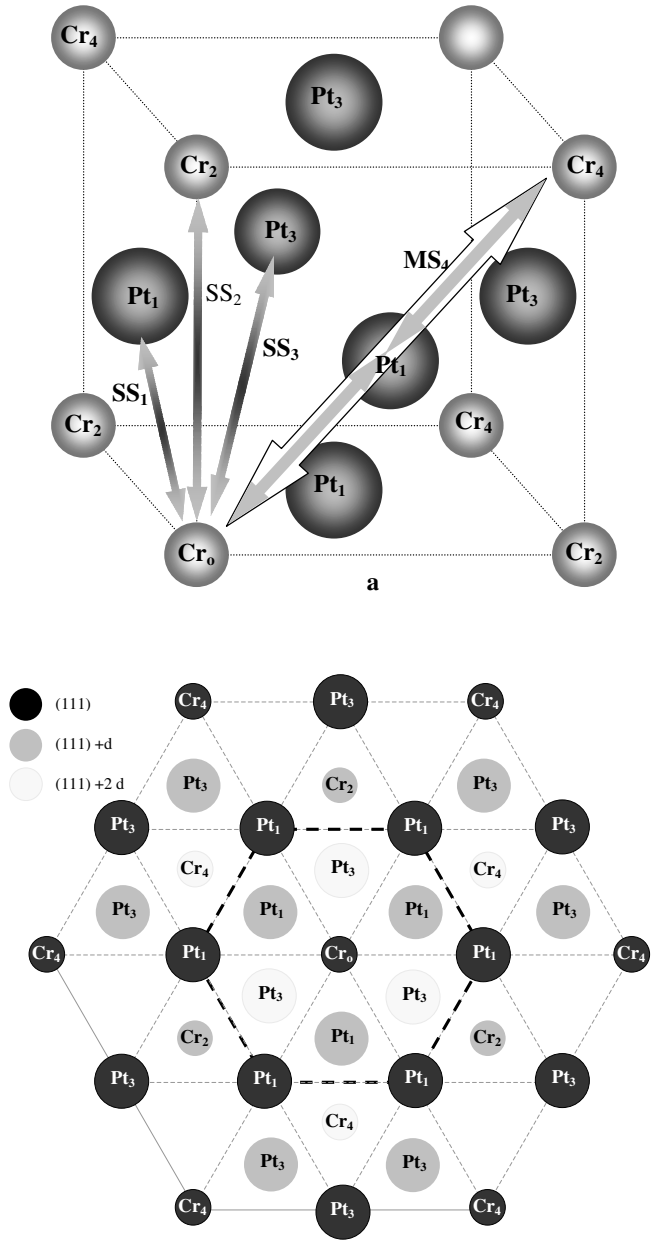

Figure 1. Upper panel: schematic view of the $L1_2$ ordered structure showing the scattering paths used in the fitting between the absorbing atom Cr_0 and the ith neighbours, Cr_i and Pt_i. Lower panel: atoms in the (111) plane (black circles) and in its upper planes at $+d_{111}$ (grey circles) and $+2d_{111}$ (white circles).

($\tilde{N}_{\parallel}^{\text{out}}$) contributions with different weights depending on the shell. Note that whatever the polarization may be, $\tilde{N}_{\parallel(\perp)}^{\text{in}} + \tilde{N}_{\parallel(\perp)}^{\text{out}}$ is equal to the total multiplicity number of the unpolarized case N_{tot}. For this reason, the XAF signals of a perfectly ordered $L1_2$-type structure or a fully chemically disordered fcc structure are independent of polarization.

Table 1. Single-scattering (SS) and multiple-scattering (MS) signals used in the calculated XAFS spectrum of the $L1_2$ ordered $CrPt_3$ fcc structure. The MS_4 signal is composed of single-(I), double-(II) and triple-(III) scattering paths. The path length is given in units of the lattice parameter a. N_{tot} is the total number of paths per absorbing atom. N^{in} is the number of independent paths per absorbing atom occurring strictly in the (111) plane while N^{out} is the number of paths out of the (111) plane. On the right side, $\tilde{N}_{\perp}^{in}$ ($_{\parallel}$) is the effective number of in-plane contributions observed in perpendicular (parallel) polarization geometry, and $\tilde{N}_{\perp}^{out}$ ($_{\parallel}$) is the effective number of out-of-plane contributions observed in perpendicular (parallel) geometry.

							Geometry			
Signal	Length (R)		N_{tot}	Scatterer(s)	N^{in}	N^{out}	$\tilde{N}_{\perp}^{in}$	$\tilde{N}_{\perp}^{out}$	$\tilde{N}_{\parallel}^{in}$	$\tilde{N}_{\parallel}^{out}$
SS_1	$a/\sqrt{2}$		12	Pt_1	6	6	0	12	9	3
SS_2	a		6	Cr_2	—	6	0	6	0	6
SS_3	$a\sqrt{3/2}$		24	Pt_3	6	18	0	24	9	15
		I	12	Cr_4	6	6	0	12	9	3
MS_4	$a\sqrt{2}$	II	24	Cr_4–Pt_1	12	12	0	24	18	6
		III	12	Pt_1–Cr_4–Pt_1	6	6	0	12	9	3

The photoelectron amplitude and phase functions were calculated using the FEFF [14] code assuming a fcc structure ($a = 3.86$ Å), as well as S_0^2 equal to 0.9 and the theoretical mean free path, $\lambda(k)$. The best fits are achieved using the FITEXA [15] program which exploits the MINUIT package [16] providing the routines for non-linear data fitting with accurate best fit statistical analysis.

3. EXAFS data analysis

This section describes the EXAFS data analysis procedures for extracting the structural parameters. The complete XAFS signals were fitted in the k-space. The out-of-plane ($400_{\perp}$ and $850_{\perp}$) data presenting higher noise (probably because of the smaller beam required in the vertical geometry) were analysed in a k-range from 2.9 to about 11 Å^{-1}. The in-plane data ($400_{\parallel}$ and $850_{\parallel}$) with better statistics were fitted over a larger k-range from 2.9 to above 12 Å^{-1}. The best fits were achieved combining signals of the $L1_2$ ordered and chemically disordered structural models as described below.

The $L1_2$-type model relies on four main contributions highlighted in figure 1 (see also table 1). Three are single-scattering contributions (SS_i) from Cr_0–Pt_1 at $a/\sqrt{2}$ (centre of the near face), Cr_0–Cr_2 at a (cube edge, SS_2) and Cr_0–Pt_3 at $a\sqrt{3/2}$ (centre of the opposite face, SS_3), respectively. The fourth (MS_4) accounts for single-(Cr_0–Cr_4) and multiple-scattering contributions from the Cr_0–Pt_1–Cr_4 ions lined up along the face diagonal, namely the double scattering from the Cr_0–Pt_1–Cr_4–Cr_0 and Cr_0–Cr_4–Pt_1–Cr_0 photoelectron paths, and the triple scattering from the Cr_0–Pt_1–Cr_4–Pt_1–Cr_0 photoelectron paths. The linear atomic arrangement strongly enhances the amplitude of multiple-scattering terms which cannot be neglected. Note that other multiple-scattering contributions, such as those from Pt_1–Cr_0–Pt_1 (linear arrangement with the Cr_0 absorber in between two Pt_1), Cr_0–Pt_1–Pt_1 (triangular configurations) and Cr_0–Pt_1–Pt_3, produced very weak signals and did not improve (or even worsened) the fitting (χ^2 and F tests).

The only contribution of the chemically disordered model is the Cr_0–Cr_1 nearest neighbour shell, since any attempt to include next neighbour contributions, such as Cr_0–Pt_2 or Cr_0–Cr_3 ones, worsen the fitting. These next neighbour contributions are probably weakened by the larger structural distortions of the disordered model and are hard to detect.

Table 2. Structural parameters corresponding to the best fits. For the in-plane geometry, the parameters characterize the in-plane neighbours (major contribution), and the parameters of the out-of-plane neighbours (minor contribution) are those extracted from the out-of-plane data weighted by the effective numbers given in table 1. In parenthesis are the errors on the last digits, calculated using the MINOS command in the MINUIT package which takes into account correlations among the parameters.

Parameters	$400_{\parallel}$	$400_{\perp}$	$850_{\parallel}$	$850_{\perp}$
a_{L1_2} (Å)	3.862(13)	3.836(19)	3.871(11)	3.852(11)
σ_1^2 (10^3 Å^2)	5.2(9)	6.2(9)	4.6(6)	4.9(11)
σ_2^2 (10^3 Å^2)	—	23.(5)	—	5.3(15)
σ_3^2 (10^3 Å^2)	8.2(12)	5.2(8)	7.9(9)	4.5(12)
σ_4^2 (10^3 Å^2)	22.(6)	21.(7)	18.(5)	17.(8)
x	—	0.69(8)	—	0.84(7)
R_{CrCr} (Å)	—	2.65(3)	—	2.70(2)
σ^2_{CrCr} (10^3 Å^2)	—	7.9(9)	—	6.9(7)
χ^2_ν	0.92	1.14	0.93	0.97

Thus, fitting out-of-plane EXAFS data requires: (i) five free parameters for the $L1_2$ model: the lattice parameter a_{L1_2} (assuming all path lengths are constrained to the fcc structure) and four Debye–Waller factors σ^2 [Note 7]; (ii) two more free parameters for the disordered model: the Cr_0–Cr_1 distance (R_{Cr-Cr}) and its related Debye–Waller factor (σ^2_{Cr-Cr}). In order to constrain the total Cr first-neighbour coordination number to 12, we refine the parameter x (table 2) that represents the fraction of Pt in the first-neighbour shell of the $L1_2$-type environment. The multiplicity number $\tilde{N}_{\perp}^{out}$ is constrained to x times the value in table 1, while the multiplicity number for the Cr–Cr nearest neighbours is constrained to a factor of $(1 - x)$. The edge energy, E_0, is left free to vary. Finally the fitting routine uses a maximum number of nine free parameters.

As already mentioned, the in-plane EXAFS data ($400_{\parallel}$, $850_{\parallel}$) result from a combination of in-plane and out-of-plane contributions. The out-of-plane contributions are included in the fitting keeping their structural parameters fixed to the values extracted from the analysis of the out-of-plane data and weighted according to table 1. Within this approach the refinement of the in-plane data gives a satisfactory best fit using only three new contributions: namely SS_1 from Cr_0–Pt_1, SS_3 from Cr_0–Pt_3 and the multiple scattering of Cr_0–Pt_1–Cr_4 configurations MS_4, while the SS_2 contribution comes only from out-of-plane atoms as sketched in figure 1. Thus, the fitting requires five free parameters: three Debye–Waller factors, the in-plane lattice parameter and the edge energy, E_0.

4. Results and discussion

Figure 2 compares the Cr K edge experimental data together with the simulated spectra obtained for a randomly disordered ('Dis') fcc structure and a $L1_2$ ordered $CrPt_3$ structure. The polarization dependence in the experimental data is rather weak for both samples. The

[7] The Debye–Waller factors for MS_4 contributions were calculated as follows: the Debye–Waller of the single-scattering term Cr_0–Cr_4, σ_4^2, was refined, the Debye–Waller of the Cr_0–Pt_1–Cr_4–Pt_1–Cr_0 triple-scattering term was calculated as $2\sigma_1^2$ (where σ_1^2 was the first shell Cr_0–Pt_1 Debye–Waller factor); finally the Debye–Waller of the double-scattering paths was calculated as $(2\sigma_1^2 + \sigma_4^2)/2$. This approximation neglects the correlation effects in the three-body distribution functions which should be taken into account for an exact treatment. However, the restricted k-range and the relatively high noise of the data would prevent a deeper insight.

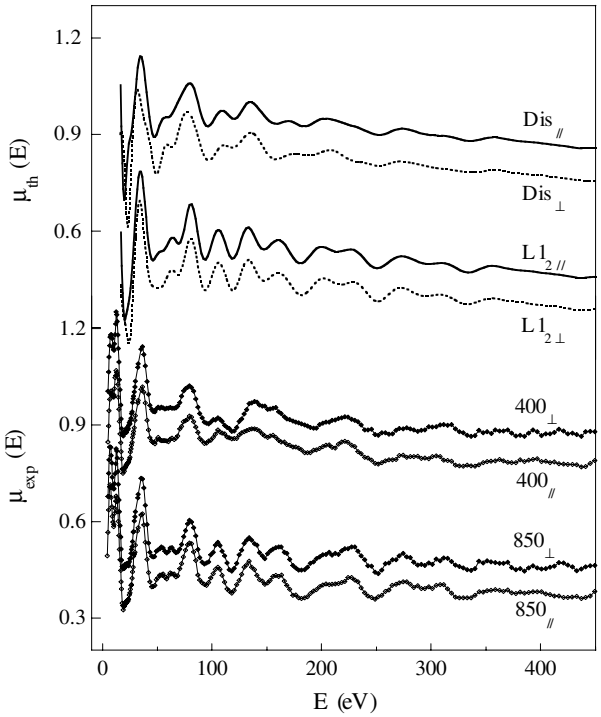

Figure 2. Experimental x-ray absorption spectra of the two $CrPt_3$ films (400 and 850 °C) for in-plane (∥) and out-of-plane (⊥) polarization geometries. For comparison, we show the simulated spectra of a randomly disordered $CrPt_3(111)$ film (Dis) and a $L1_2$ ordered $CrPt_3(111)$ film ($L1_2$) for both polarizations. The curves are shifted for clarity.

great weakness of the polarization effect observed in the simulated XAFS spectra is due to the limited size of the model clusters used ($R_{max} = 6$) and the not perfectly isotropic disordered model. The $L1_2$ ordered model reproduces the main features of the experimental spectra of the ordered film, thus confirming the x-ray diffraction results which pointed to a high degree of $L1_2$ long range order. Comparing the $400_{\parallel}$ and $400_{\perp}$ spectra would suggest an intermediate behaviour between the Dis and $L1_2$ models.

The moduli of the Fourier transform (|FT|) of the k-weighted experimental and simulated XAFS spectra are shown in figure 3. The main peak (in the R-region between 1 and 3.5 Å) mainly derives from nearest neighbour correlations (Cr–Pt around 2.7 Å in the $L1_2$ structure). Let us mention that the Pt scatterers lead to an asymmetric |FT| peak with an evident shoulder in the high R-region. This splitting is typical for heavy back-scatterers as previously observed in $CoPt_3$ films [5]. The second peak (located between 3.5 and 5.5 Å in figure 3) is dominated by multiple-scattering effects from Cr–Pt–Cr chains lined up along the cube face diagonal (see figure 1). The similarity between the |FT| of the 850 °C data and the $L1_2$ model is well marked. In contrast, the in-plane and out-of-plane |FT|s for the film grown at 400 °C look like those of the Dis and $L1_2$ models respectively. The pronounced polarization dependence in the 400 °C sample definitively indicates some anisotropy in the Cr local order.

Refining the out-of-plane data under the hypothesis of $L1_2$ ordered structure ($x = 1$) gives a poor agreement, expressed by the values of reduced χ^2 equal to 1.9 and 1.5 for the $400_{\perp}$ and $850_{\perp}$ data sets, respectively. Adding a Cr–Cr nearest neighbour contribution significantly improves the quality of the fit with $\chi^2_\nu(400_{\perp}) \sim 1.1$ and $\chi^2_\nu(850_{\perp}) \sim 1$.

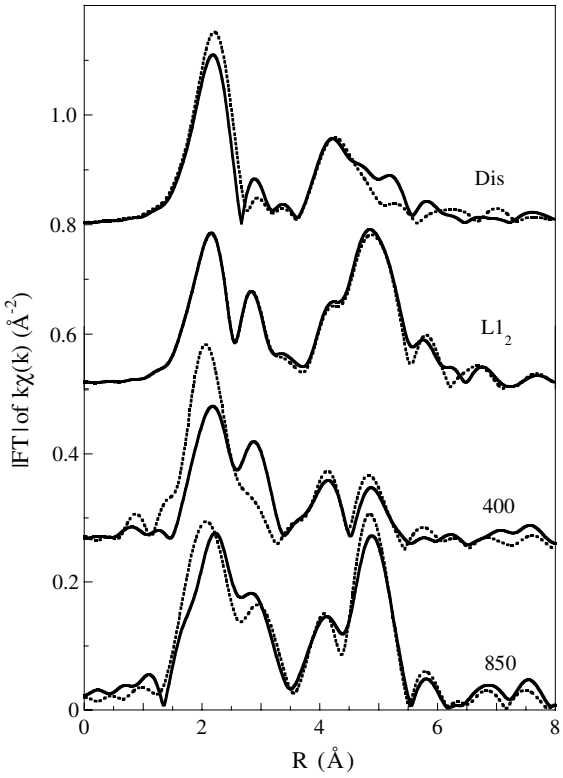

Figure 3. Moduli of Fourier transforms (|FT|) of the experimental and simulated $k\chi(k)$ spectra (k-range: 2.9–10.5 Å^{-1}) presented in figure 2 for the two geometries: $\parallel$ (solid lines) and $\perp$ (dashed lines).

The best fits of the in-plane data have a reduced χ^2_ν slightly better than 1 (table 2). Statistical analysis (F test) has shown that adding a Cr–Cr nearest neighbour contribution (disordered sites) does not improve the fitting while x systematically increases above 0.96. Since this Cr–Cr contribution is too weak to be reliably refined, the parameters R_{CrCr} and σ^2_{CrCr}, were kept fixed consistently with the out-of-plane data and the x values corresponding to only Cr–Cr out-of-plane pairs were thus fixed to 0.96 and 0.92 for the 850 and 400 °C samples respectively.

The structural parameters derived from the best fits are summarized in table 2. The error bars on the parameters have been calculated using the MINOS command of the MINUIT package [16] which takes into account the correlations between the parameters. The best fits are presented in figure 4. For the 850 °C sample figure 5 shows the partial contributions used in the analysis. The |FT|s of the experimental and best fitted spectra calculated in the same k-range, 2.9–10.5 Å^{-1}, are shown in figure 6. For comparison, the lower panel of figure 6 shows the |FT| of the $400_\perp$ and $850_\perp$ simulated spectra obtained without Cr–Cr nearest neighbour correlations (i.e. using only the $L1_2$ ordered model contributions), indicating clearly the poorer fitting.

Table 2 demonstrates a polarization dependence of the lattice parameter a_{L1_2} with the out-of-plane parameter shorter than the in-plane one, indicating a fcc packing compressed along the [111] direction, normal to the film plane. This distortion decreases from 0.8 to 0.5% when the growth temperature increases from 400 to 850 °C. Note that the constraint

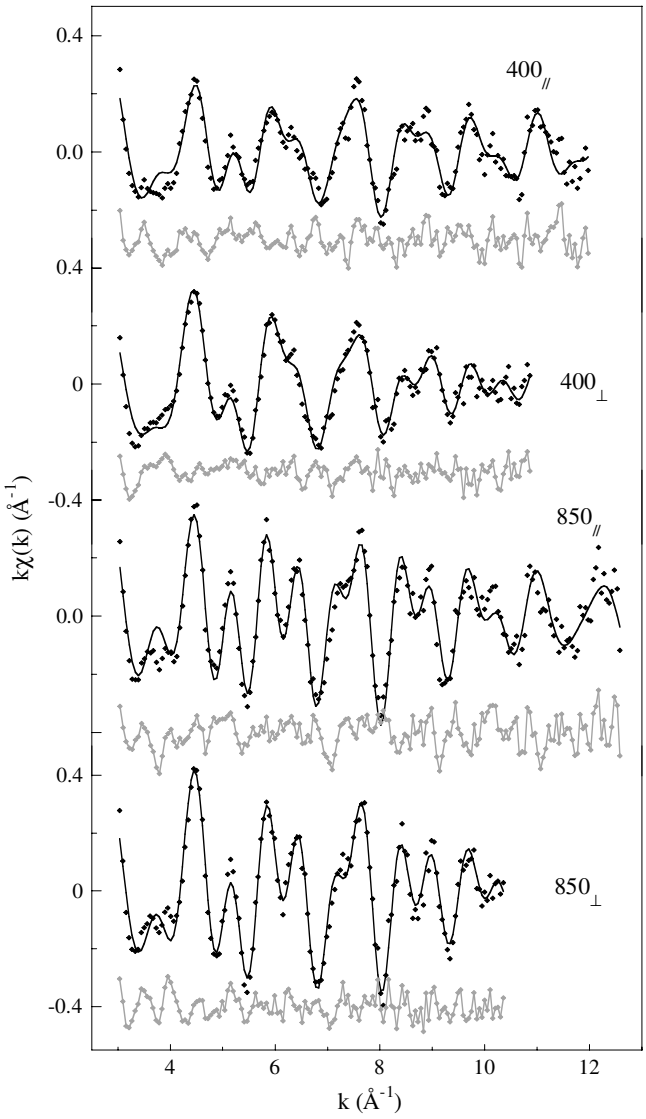

Figure 4. Experimental (dots) and best fitted (solid lines) $k\chi(k)$ spectra of two $CrPt_3$ films grown at 400 and 850 °C, for in-plane (∥) and out-of-plane (⊥) polarizations. For each fit the residual $k\chi(k)_{\mathrm{exp}} - k\chi(k)_{\mathrm{fit}}$ is shown by a grey line.

imposed in the fitting procedure gives a high sensitivity to the differences between in-plane and out-of-plane lattice parameters. This deformation is in agreement with our previous x-ray measurements [7]; however, the XAFS parameters are shorter than those deduced from the interatomic distances measured by means of x-rays: for the 850 °C sample, the d_{111} and d_{220} distances lead to out-of-plane and in-plane parameters equal to 3.87 and 3.88 Å, very close to the value for the bulk phase, equal to 3.876 Å [17]. However, it must be noticed that a discrepancy between XAS and XRD results is often reported in the literature. It can be either a fictitious effect, due to the correlation between distances and energy scale parameters in the EXAFS formula, or a physical result due to anharmonicity effects which cause the

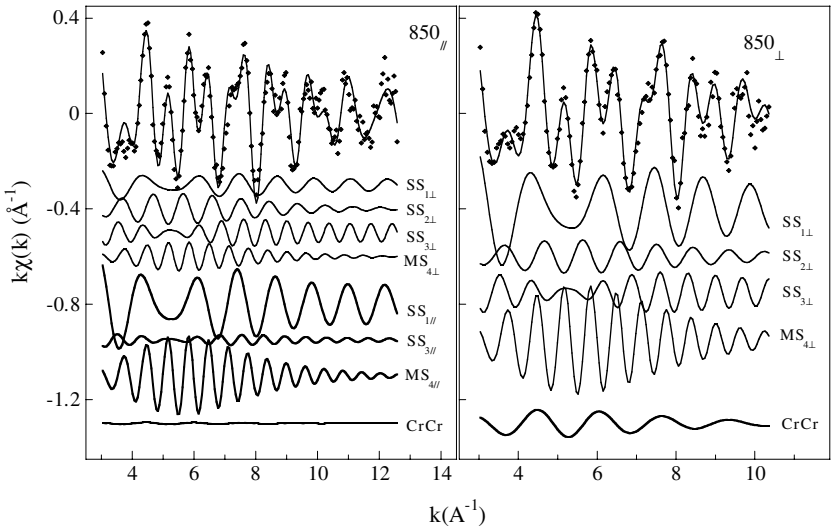

Figure 5. Best fits obtained for the 850 °C sample in the two experimental geometries shown with their partial contributions (shifted for clarity): in ∥ geometry, the out-of-plane contributions are those derived from the analysis of the out-of-plane spectra weighted according to table 1. The multiple-scattering partial contributions (MS) are a combination of single-, double-and triple-scattering terms as described in the text.

deviation of local atomic distributions from the simple Gaussian approximation assumed in the derivation of the standard EXAFS formula (1). Deviation from a Gaussian distribution can be treated including a higher cumulant expansion in the equation (1) as described well in [18] and references therein. However, a reliable cumulant analysis requires good XAS data over a large k-range with a very good signal to noise ratio; that is not the present case.

The local structure in the 400 °C sample is systematically more disordered (higher Debye–Waller factors) than in the 850 °C one. In both films, the Cr–Cr nearest neighbour distances are shorter and more spread out (indicated by a larger $\sigma^2_{\mathrm{Cr-Cr}}$) than the Cr–Pt ones equal to $\frac{a_{\mathrm{L1_2}}}{\sqrt{2}}$. The application of equation (2) for the nearest neighbours in a fcc environment leads to the following simple relations between the true coordination number (N^{in} or N^{out}) and the measured polarization-dependent coordination number ($\tilde{N}_j$):

$$\begin{aligned} \tilde{N}_{\parallel} &= 1.5N^{\mathrm{in}} + 0.5N^{\mathrm{out}} \\ \tilde{N}_{\perp} &= 2N^{\mathrm{out}}. \end{aligned} \tag{3}$$

The numbers of Cr–Cr correlations lying out of the film plane, $N^{\mathrm{out}}_{\mathrm{Cr-Cr}}$, are ≈1.8 and 1 for the 400 and 850 °C samples, respectively. In contrast, in the plane only Pt nearest neighbours are firmly found for both samples. Therefore, even in the film grown at 400 °C, for which long range chemical order is absent, a high degree of $\mathrm{L1_2}$-type local order exists and is clearly anisotropic. Such anisotropy is also observed in the 850 °C sample, but less pronounced. The fraction of out-of-plane Cr–Cr nearest neighbours decreases from about 30% in the 400 °C sample to about 15% in the 850 °C sample. It is worth mentioning that an in-plane local chemical ordering similar to that found in the 400 °C sample was also proposed to explain the diffuse intensity in the RHEED patterns observed during annealing of a $[\mathrm{Cr(2\ \AA)/Pt(7\ \AA)}]_{19.5}$ superlattice around 400 °C [7].

The total number of Pt nearest neighbours around a Cr atom, $N_{\mathrm{Pt}} \sim 10.2$ in the 400 °C sample and 11 in the 850 °C sample, can be compared to that deduced from the long range

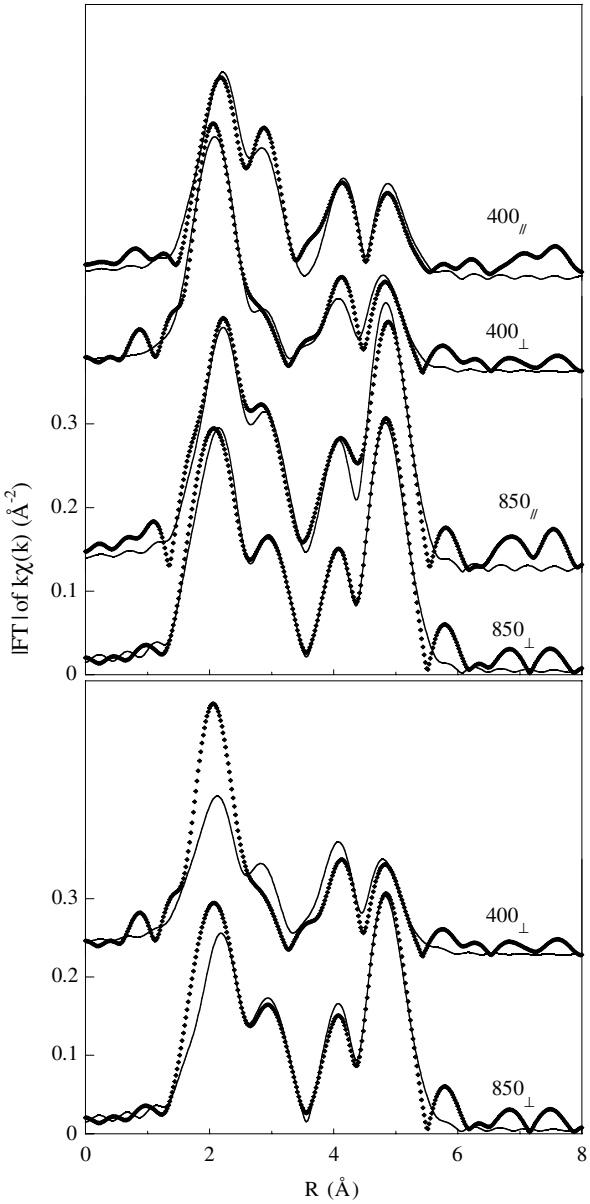

Figure 6. In the upper panel: experimental (open diamonds) and best fitted (solid lines) |FT| curves of the two $CrPt_3$ films for in-plane (∥) and out-of-plane (⊥) polarizations. In the lower panel: best fits (solid lines) of the out-of-plane polarization Fourier transforms assuming a perfect $L1_2$-type order.

order parameter S determined by x-ray diffraction measurements as shown in the following paragraph.

The $L1_2$ structure is represented by four interpenetrating cubic sublattices: three are equivalent and constructed from the centres of two opposite faces in the fcc lattice (sublattices β) and the fourth consists of the corners of the fcc lattice (sublattice α). Therefore, an atom

on the sublattice α has only first neighbours on the sublattice β, and an atom on the sublattice β has 1/3 first neighbours on α and 2/3 on β, respectively. S is then defined as $P^{\alpha}_{\mathrm{Cr}} - P^{\beta}_{\mathrm{Cr}}$, where P^{α}_{Cr} and P^{β}_{Cr} are the rates of occupancy of the sublattices α and β by Cr atoms. These two occupancy rates are related to the Cr atomic fraction, X_{Cr}, and the ratio, ν, of the number of sites belonging to the sublattice α to the total number of sites in the fcc lattice ($\nu = 1/4$ in this case) as follows:

$$\nu P^{\alpha}_{\mathrm{Cr}} + (1-\nu) P^{\beta}_{\mathrm{Cr}} = X_{\mathrm{Cr}}. \tag{4}$$

Moreover, the sum of the rates of occupancy of a sublattice α by Cr and Pt atoms is equal to 1, i.e. $P^{\alpha}_{\mathrm{Cr}} + P^{\alpha}_{\mathrm{Pt}} = 1$; the same relation holds for the sublattice β.

Assuming a random distribution of atoms on anti-sites (i.e. Cr on site β or Pt on site α) and considering only short range correlations, the probability of finding one Pt nearest neighbour around a Cr atom is given by

$$P^{\mathrm{CrPt}} = \frac{\nu}{X_{\mathrm{Cr}}} P^{\alpha}_{\mathrm{Cr}} P^{\beta}_{\mathrm{Pt}} + \frac{1-\nu}{X_{\mathrm{Cr}}} P^{\beta}_{\mathrm{Cr}} \left(\frac{2}{3} P^{\beta}_{\mathrm{Pt}} + \frac{1}{3} P^{\alpha}_{\mathrm{Pt}} \right). \tag{5}$$

Finally, using the different relations between the four occupancy rates, N_{Pt} (equal to $12 P^{\mathrm{Cr-Pt}}$) is simply related to the LRO parameter S by: $N_{\mathrm{Pt}} = 9 + 3S^2$. For the 850 °C sample, the value of S deduced from the x-ray measurements [7], equal to 0.95, leads to a number of Pt nearest neighbours equal to 11.7, slightly larger than that deduced from the XAFS measurements.

In summary, we have found in both $CrPt_3$ films a strong chemical local order with only Cr–Pt nearest neighbour correlations in the film plane. A few Cr–Cr nearest neighbour correlations are firmly extracted only from the out-of-plane polarization data. Their number decreases by a factor of two in the 850 °C sample exhibiting long range ordering. Such anisotropic chemical local order is completely different from that found in $CoPt_3$ films grown at 400 °C where a 2D segregation of Co atoms in the film plane was proposed to explain the strong magnetic perpendicular anisotropy. It was proposed that the larger number of in-plane Co–Co correlations was promoted by the segregation of the bigger atoms of Pt at the advancing surface during the co-deposition process. In the $CrPt_3$ films, we believe that Pt segregation is highly reduced due to stronger interactions between Cr and Pt atoms, which would favour a lateral local order. This idea is supported by both the higher bulk order–disorder transition temperature of the $CrPt_3$ $L1_2$ phase of 1066 °C and its smaller activation energy for an ordering process equal to 0.6 eV/atom,[8] compared to the values for the $CoPt_3$ alloy (695 °C and 3.1 eV/atom [19]).

5. Conclusion

Polarized XAFS measurements performed on $CrPt_3$(111) films have revealed an enhancement of the local chemical order in the (111) film plane. The number of Cr–Cr nearest neighbour correlations found only out-of-film-plane decreases with the degree of $L1_2$-type long range order. Even in the film grown at 400 °C which exhibits no LRO, a number of in-plane Pt nearest neighbours around a Cr atom very close to 6 is found, which is quite different to results reported on $CoPt_3$ films. It is suggested that the observed behaviour for $CrPt_3$ results from strong interactions between Cr and Pt atoms stemming from a profound Cr(3d)–Pt(5d) band structure hybridization. Through this hybridization, the spin–orbit coupling of Pt affects the orbital moment of Cr, leading to a violation of the Hund's third rule characterized by an orbital moment on Cr which is parallel to its spin moment, as found by relativistic energy band calculations [9]. For the $CrPt_3$ film grown at 850 °C, it is hardly credible that the perpendicular

[8] The activation energy was deduced assuming an Arrhenius behaviour of the LRO chemical order parameter, S, determined in the $CrPt_3$ films [7].

magnetic anisotropy developed by this film [7] ($K_{\text{eff}} = 0.23$ MJ m^{-3}) originates from the residual in-plane tensile stress estimated at 0.3 GPa (using an elastic constant of 110 GPa [20] and a lattice deformation of -0.3%). Indeed, assuming a negative magnetostriction constant of $\sim -2 \times 10^{-4}$, such a stress would lead to a magnetoelastic anisotropy energy of only 0.07 MJ m^{-3}. Therefore, the ferromagnetic coupling between Cr–Cr atoms, lined up along the $\langle 001 \rangle$ directions oriented out of the film plane, would favour an easy axis of magnetization perpendicular to the film plane.

Acknowledgment

In Konstanz, this project was funded by the Deustche Forschungsgemeinshaft (SFB 513), which is gratefully acknowledged.

References

[1] Weller D, Brändle H, Gorman G L, Lin C J and Notarys H 1992 *Appl. Phys. Lett.* **61** 2726
[2] Farrow R F C, Weller D, Marks R F, Toney M F, Cebollada A and Harp G R 1996 *J. Appl. Phys.* **79** 5967
[3] Shapiro A L, Rooney P W, Tran M Q, Hellman F, Ring K M, Kavanagh K L, Rellinghaus B and Weller D 1999 *Phys. Rev.* B **60** 12826
[4] Maret M, Cadeville M C, Herr A, Poinsot R, Beaurepaire E, Lefebvre S and Bessière M 1999 *J. Magn. Magn. Mater.* **191** 61
[5] Meneghini C, Maret M, Parasote V, Cadeville M C, Hazemann J L, Cortes R and Colonna S 1999 *Eur. Phys. J.* B **7** 347
[6] Grange W, Maret M, Kappler J P, Vogel J, Fontaine A, Petroff F, Krill G, Rogalev A, Goulon J, Finazzi M and Brookes N 1998 *Phys. Rev.* B **58** 6298
[7] Maret M, Albrecht M, Köhler J, Poinsot R, Uhlaq-Bouillet C, Tonnerre J M, Berar J F and Bucher E 2000 *J. Magn. Magn. Mater.* **218** 151
[8] Leonhardt T D, Chen Y, Rao M, Laughlin D E, Lambeth D N and Kryder M H 1999 *J. Appl. Phys.* **85** 4307
[9] Oppeneer P M, Galanakis I, Grechnev A and Eriksson O 2002 *J. Magn. Magn. Mater.* **240** 371
[10] Hellwig O, Weller D, Kellock A, Baglin J and Fullerton E 2001 *Appl. Phys. Lett.* **79** 1151
[11] Lee P A, Citrin P H, Eisenberger P and Kinkaid B M 1981 *Rev. Mod. Phys.* **53** 769
[12] Revenant-Brizard C, Regnard J R, Mimault J, Duclos D and Faix J 1997 *J. Physique Coll.* **7** C2 325
[13] Stern E A 1974 *Phys. Rev.* B **10** 3027
[14] Zabinsky S I, Rehr J J, Ankudinov A, Albers R C and Eller M J 1995 Multiple scattering calculations of x-ray absorption spectra *Phys. Rev.* B **52** 2995
[15] Meneghini C, Bardelli F and Mobilio S, unpublished
[16] 1994minuit James F 1994 *MINUIT: Function Minimization and Error Analysis. Reference Manual—V 94.1* Program Library D506, CERN
[17] Villars P and Calvert L D 1985 *Pearson's Handbook of Crystallographic Data for Intermetallic Phases* vol 2 (Cleveland, OH: American Society for Metals)
[18] Fornasini P, Beccara S A, Dalba G, Grisenti R, Sanson A, Vaccari M and Rocca F 2004 *Phys. Rev.* B **70** 174301
[19] Dahmani C E, Cadeville M C and Pierron-Bohnes V 1985 *Acta Metall.* **3** 369
[20] Maret M, Gilles B, Simon J P, Verdier M, Guhr I, Riedlinger B, Albrecht M and Schatz G 2005 *J. Cryst. Growth* **275/1-2** 2289